1998 *Biochemistry* **2010,** *49,* 1998–2007
DOI: 10.1021/bi901674q

BIOCHEMISTRY
including biophysical chemistry & molecular biology
Article

The Rate-Limiting Catalytic Steps of Hydroxymandelate Synthase from *Amycolatopsis orientalis*[†]

Panqing He, John A. Conrad, and Graham R. Moran*

Department of Chemistry and Biochemistry, University of Wisconsin—Milwaukee, 3210 North Cramer Street, Milwaukee, Wisconsin 53211-3029

Received September 24, 2009; Revised Manuscript Received January 7, 2010

ABSTRACT: Hydroxymandelate synthase (HMS) catalyzes the committed step in the formation of *p*-hydroxyphenylglycine, a recurrent substructure of polycyclic nonribosomal peptide antibiotics such as vancomycin. HMS has the same structural fold as and uses the same substrates as 4-hydroxyphenylpyruvate dioxygenase (HPPD) (4-hydroxyphenylpyruvate (HPP) and O_2). Moreover, HMS catalyzes a very similar dioxygenation reaction to that of HPPD, adding the second oxygen atom to the benzylic position, rather than the aromatic C1 carbon of the substrate. The dissociation constant for HPP (59 μM) was measured under anaerobic conditions by titrating substrate with enzyme and monitoring the intensity of the weak ($\varepsilon_{475nm} \sim 250\ M^{-1}\ cm^{-1}$) charge-transfer absorption band of the HMS·Fe(II)·HPP complex. Pre-steady-state analysis indicates that evidence exists for the accumulation of three intermediates in a single turnover and the decay of the third is rate-limiting in multiple turnovers. The rate constants used to fit the data were $k_1 = 1 \times 10^5\ M^{-1}\ s^{-1}$, $k_2 = 250\ s^{-1}$, $k_3 = 5\ s^{-1}$, and $k_4 = 0.3\ s^{-1}$. However, the values for k_1 and k_2 could not be accurately measured due to both a prolonged mixing time for the HMS system that obscures observation at the early times (< 10 ms) and the apparent high relative value of k_2. The third phase, k_3, is attributed to the formation of the product complex, and no kinetic isotope effect was observed on this step when the protons of the substrate's benzylic carbon were substituted with deuteriums, suggesting that hydroxylation is fast relative to the steps observed. The final and predominantly rate-limiting step shows a 3-fold decrease in the magnitude of the rate constant in deuterium oxide solvent, and a proton inventory for this step suggests the contribution of a single proton from the solvent environment.

Vancomycin was adopted into therapeutic use some 40 years ago in response to new strains of staphylococci that were growing resistant to penicillin. Despite known resistance, particularly among enterococci, vancomycin has remained a "last line of defense" drug able to treat infections that defy response to multiple antibiotics (*1*, *2*). One of the key substructures of a number of macrocyclic peptide antibiotics, including vancomycin, chloroemomycin, and complestatin, is *p*-hydroxyphenylglycine (PHPG).[1] PHPG is derived in four enzymatic steps from tyrosine. Hydroxymandelate synthase (HMS) catalyzes the first and committed step of this sequence, the conversion of 4-hydroxyphenylpyruvate (HPP) to hydroxymandelate (HMA) (Scheme 1).

HMS catalyzes a similar reaction to that of 4-hydroxyphenylpruvate dioxygenase (HPPD). The difference between the two reactions is the carbon to which one of the atoms of dioxygen is directed. In the case of HPPD, hydroxylation occurs on the aromatic ring, inducing an NIH shift of an aceto substituent to an adjacent aromatic carbon; HMS instead hydroxylates the benzylic carbon (Scheme 1). The primary sequences of HPPD and HMS have ~30% identity, and the two enzymes share the same tertiary fold (*3*). However, while HPPD has been studied quite extensively (*4*), HMS is a relatively recent addition to the scientific literature (*3*, *5*, *6*). We have expressed and purified HMS from *Amycolatopsis orientalis* and conducted a series of experiments designed to define the salient details of catalysis in regard to substrate binding, oxygen reactivity, and rate-limiting catalytic processes.

MATERIALS AND METHODS

Materials. The sodium salt of HEPES buffer, monobasic and dibasic potassium phosphate, 99.8 atom % deuterium oxide, and β-mercaptoethanol (βME) were purchased from ACROS. Ammonium sulfate, sodium chloride, Luria−Bertani media (LB), and streptomycin sulfate were purchased from Fisher Scientific. Isopropyl β-thiogalactopyranoside (IPTG) was from United States Biochemicals. Ferene S (3-(2-pyridyl)-5,6-bis(2-[5-furylsulfonic acid])-1,2,4-triazine), ampicillin, and HPP were purchased from Sigma-Aldrich Co. Sephacryl S-200 was purchased from Amersham and Q-Sepharose from Bio-Rad. Electrophoretic grade agarose was purchased from ICN Biomedicals, Inc. Chemically competent *Escherichia coli* TOP10 and BL21 DE3 cells were obtained from Invitrogen. The pET17b plasmid was purchased from Novagen. The Midiprep plasmid preparation kit and Qiaquick gel extraction kit were from Qiagen. Restriction enzymes *Nde*I and *Xho*I and T4 DNA ligase were purchased from New England Biolabs. Ten kilodalton nominal molecular weight limit (NMW) Biomax centrifugal filters were manufactured by Amicon. The apo form of HMS was expressed and purified as previously described (*3*, *7*).

[†]This research was supported a National Science Foundation grant to G.R.M. (MCB0843619) and by a UWM Research Growth Initiative Grant to G.R.M.

*To whom correspondence should be addressed. Phone: (414) 229-5031. Fax: (414) 229-5530. E-mail: moran@uwm.edu.

[1]Abbreviations: HMS, hydroxymandelate synthase; HPPD, (4-hydroxyphenyl)pyruvate dioxygenase; HMA, hydroxymandelate; HPP, (4-hydroxyphenyl)pyruvate; HG, homogentisate; PHPG, *p*-hydroxyphenylglycine; βME, β-mercaptoethanol; HEPES, *N*-(2-hydroxyethyl)piperazine-*N*′-2-ethanesulfonic acid; NMWL, nominal molecular weight limit; PMT, photomultiplier tube; PDA, photodiode array; NMR, nuclear magnetic resonance.

 Published on Web 01/29/2010

Scheme 1: Catalytic Chemistries of HMS and HPPD

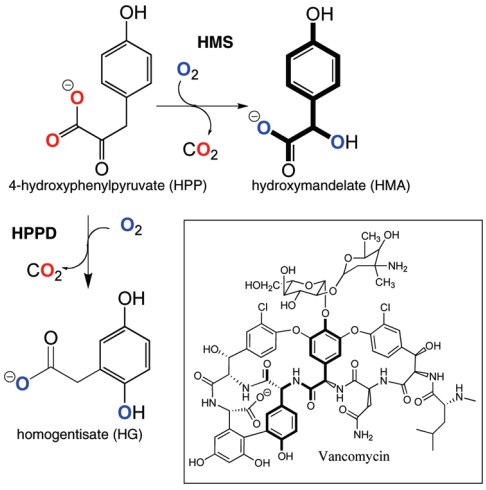

Extinction Coefficients. The extinction coefficient of apo-AoHMS was calculated to be 20525 M^{-1} cm^{-1} at 280 nm by the method of Pace (*8*). The molar extinction coefficient of HPP was 3400 M^{-1} cm^{-1} at 276 nm at pH 7.0 (*9*). The molar extinction coefficient of HMA was 1280 M^{-1} cm^{-1} at 274 nm and was determined using an internal standard, nuclear magnetic resonance (NMR) method described by Johnson-Winters et al. (*9*).

Enzyme Assays and Steady-State Observations. HMS activity was measured using a Hansatech Oxygraph dioxygen electrode. Standard activity assays included 1 μM enzyme, 1 mM βME, 10 μM Fe(II), and 300 μM HPP in 20 mM HEPES, pH 7.0 at 5 °C, with atmospheric oxygen (~390 μM). Reactions were initiated with HPP once the background rate of dioxygen consumption had been assessed. Background depletion of dioxygen results from the free and enzyme-bound forms of the added metal ion cycling between ferrous and ferric forms in the presence of dioxygen and the βME reductant. Enzymatic rates were measured between 20 and 50 s after initiation and were corrected for background dioxygen reduction. Steady-state kinetic parameters were determined at 5 °C for direct comparison with pre-steady-state experiments conducted at the same temperature. Where possible, apparent kinetic parameters were measured by varying the concentration of HPP or O_2 in assays that contained high concentrations of the other substrate. Data were fit to the Michaelis−Menten equation (eq 1).

$$v = V_{max}[S]/(K_m + [S]) \quad (1)$$

Measurement of the Dissociation Constant for the HMS·Fe(II)·HPP Complex. The binding constant for the HMS·Fe(II)·HPP complex was measured under anaerobic conditions according to the methods of Johnson-Winters et al. (*7*). The concentration of the HPPD·HPP complex was plotted against total HPP concentration. These data were fit to eq 2 in which the K_{dHPP} value and the concentration of available binding sites ([HPPD]) were obtained.

$$[HPPD\cdot HPP] = \{K_{dHPP} + [HPP] + [HPPD] - ((K_{dHPP} + [HPP] + [HPPD])^2 - 4[HPP][HPPD])^{1/2}\}/2 \quad (2)$$

Product Analysis for HPP. The propensity of HMS to hydroxylate the benzylic carbon as opposed to the aromatic C1 position was measured using HPLC analysis of multiple turnover reaction mixtures. Assays included 2 μM enzyme, 1 mM βME, 10 μM Fe(II), and 25−100 μM HPP in 20 mM HEPES, pH 7.0 at 25 °C, with atmospheric oxygen (~250 μM) and were monitored using a dioxygen electrode. Each reaction was allowed to proceed until the HPP substrate was entirely consumed and the rate of oxygen consumption returned to the background rate observed prior to the initiation of the reaction. The reaction mixture was then withdrawn (700 μL) and immediately mixed with trichloroacetic acid (TCA) (300 μL of 10% (w/v)) to precipitate HMS and stabilize any HG formed in the reaction. The acidified reaction mixture was then centrifuged at 20000*g* for 10 min and the supernatant injected (50 μL) onto an analytical Phenomenex phenyl HPLC column (4.6 × 250 mm) coupled to a Waters 600E HPLC pump. The mixture was separated isocratically at 1 mL/min with a mobile phase of 20 mM citrate, pH 3.5 (95%), and acetonitrile (5% v/v). HG and HMA were detected at their absorbance maxima (290 and 274 nm, respectively) using a Waters 2487 dual-wavelength detector. Standard curves for HMA and HG were prepared from the authentic compounds by serial dilution, acidification to 3% (w/v) TCA, and HPLC detection under the same conditions.

Preparation of 3′,3′-Dideuterio-HPP. The protons of the benzylic carbon of HPP were exchanged for solvent deuteriums by taking advantage of the tautomerization reaction that reversibly takes HPP from the keto to the enol form. The purpose of this was to use the dideuterium-labeled substrate to perturb the hydroxylation reaction that occurs at the benzylic carbon during the formation of HMA. The exchange process was monitored using a 500 MHz Bruker NMR spectrometer. The loss or accumulation of integration of the resonances for benzylic protons at 3.9 ppm was used to determine rate constants for the exchange reaction.

The exchange of solvent deuteriums for substrate protons was carried out at 25 °C. HPP (30 μL of 60 mM) was added to 660 μL of 200 mM phosphate-buffered deuterium oxide, pD 7.0. The exchange of solvent protons for substrate deuteriums was measured at 5 °C in order to define the rate constants for this process at the temperature of kinetic experiments conducted in H_2O. 3′,3′-Dideuterio-HPP (45 μL of 48.4 mM) was added to 655 μL of 200 mM phosphate buffer, pH 7.0. In each case, the measured integration values were plotted against time of initial free induction decay acquisition and fit to a linear combination of two exponentials for the initial formation of the 3′-protio-3′-deuterio-HPP and its subsequent decay to either 3′,3′-dideuterio- or 3′,3′-diprotio-HPP.

External Chemical Quench and Product Analysis. The level of HMA made at various time points in a single turnover of HMS was measured using an Update Instruments System 1000 chemical/freeze quench apparatus, followed by HPLC detection. The HMS·Fe(II)·HPP complex was prepared in an anaerobic glovebox, transferred to the quench apparatus syringe, and capped. This was then taken out of the glovebox, mounted to the quench instrument, and mixed with an equal volume of oxygenated, pH 7.0, 50 mM phosphate buffer at 6 °C. Prior to mixing, the enzyme complex contained 495 μM HMS, 487 μM Fe(II), 3.1 mM HPP, and 601 μM 2,5-dihydroxybenzoate (DHB) as an internal standard in 50 mM phosphate, and the oxygenated buffer contained 480 μM O_2. Each ~200 μL of reaction was quenched with ~100 μL of 30% TCA, at specified age times. The quenched reactions were centrifuged for 20 min at 12000*g* to pellet the precipitated enzyme.

The supernatant (40 μL) was injected onto a Phenomenex Synergi phenyl column (250 × 4.6 mm) run isocratically at

1 mL/min with a solution consisting of 98% 20 mM citric acid, pH 3.5, and 2% acetonitrile, and the elution was monitored at 274 nm (λ_{max} of HMA) and 340 nm (near λ_{max} for DHB and a shoulder for keto-HPP). The concentrations of the internal standard DHB and the reaction product HMA at each age time were determined by comparison to standard curves prepared from DHB and HMA that spanned the range of 10−500 μM in each case. Two reactions were quenched and analyzed for each time point and averaged. Control reactions involving the same enzyme sample, mixed against anaerobic, pH 7.0, and 50 mM phosphate buffer (15 min bubbling with argon), were run initially to quantify enzyme complex oxidation that is part of the sample preparation process, which produces a base level of HMA. This level did not differ from the HMA level observed in reactions quenched at the theoretically fastest time point of 2.5 ms. Subsequently, 2.5 ms reactions were used as the control. They were run as part of each set of time point collection, and the HMA detected for the 2.5 ms reaction was subtracted from that detected at all later time points.

Stopped-Flow Measurements. Transient state kinetics were measured using a Hi-Tech (now TgK) Scientific DX2 stopped-flow instrument. When required, dissolved molecular oxygen was removed from the instrument enzymatically by introducing an anaerobic solution of glucose (50 mM) and glucose oxidase (20 units/mL) 15 h prior to experiments.

Holoenzyme oxidation was measured as previously described (*7*). An anaerobic holoenzyme complex (10 μM final) was mixed against varied pseudo-first-order concentrations of dioxygen (335−933 μM final). Rate constants (k_{obs}) were determined from the fit of the increase in absorbance at 310 nm, which is associated with the oxidation of the active site ferrous ion, to a single exponential, and these were plotted against dioxygen concentration ([O_2]). The data obtained were fit to eq 3 to determine the magnitude of the second-order rate constant for holoenzyme oxidation (k).

$$k_{obs} = k[O_2] \tag{3}$$

The reaction of the HMS·Fe(II)·HPP complex with dioxygen was monitored using both single-wavelength photomultiplier detection and multiple-wavelength photodiode array detection (PMT and PDA). Hereafter, wherever unspecified as diprotio or dideuterio, "HPP" by itself refers to the diprotio species. The essential experiments involving regular diprotio-HPP in H_2O as well as all experiments involving dideuterio-HPP had components with these final concentrations: 99 μM HMS, 85 μM Fe(II), 1340 μM HPP (or dideuterio-HPP), and 80 μM O_2. All D_2O, proton inventory, and pH experiments involving diprotio-HPP had the following final component concentrations: 160 μM HMS, 150 μM Fe(II), 1470 μM HPP, and 145 μM O_2. The buffer in all cases was 20 mM HEPES, pH 7.0.

The HMS·Fe(II)·HPP complex was made anaerobic according to previously described methods by subjecting apo-HMS, Fe(II), and HPP in segregated compartments of a tonometer to 45 cycles of vacuum and argon at 5 °C and then combining each of the components (*9*). The complex made was then reacted with molecular oxygen on the stopped-flow instrument maintained at 5 °C, and the reactions were observed spectrophotometrically. Data were collected with logarithmic time spacing. They were rendered and analyzed using the Specfit/32 Global Analysis System (Spectrum Software Associates, Chapel Hill, NC) and fit to the four-step model depicted in Scheme 2 that assumes rapid reacquisition of the excess substrate at the end of turnover.

Scheme 2: The Four-Step Model Used To Fit HMS's Single Turnover Reactions

$$\text{HMS.Fe(II).HPP} + O_2 \xrightarrow{k_1} \text{Intermediate I}$$

$$\text{Intermediate I} \xrightarrow{k_2} \text{Intermediate II}$$

$$\text{Intermediate II} \xrightarrow{k_3} \text{Intermediate III}$$

$$\text{Intermediate III} \xrightarrow{k_4} \text{HMS.Fe(II).HPP} + \text{HMA} + CO_2$$

For experiments that used deuterium oxide, the HMS solvent was exchanged using repeated centrifugal concentration with an Amicon 10 kDa NMWL filter device, followed by subsequent dilution in a HEPES-buffered D_2O/H_2O mixture, pD/H 7.0, to achieve an ~99.9% exchange of solvent. The results from the proton inventory experiments were fit to eqs 4a−4c.

$$k_n/k_0 = \sum_{i=1}^{x}(1 - n + n\phi^T) \tag{4a}$$

$$k_n/k_0 = (1 - n + n\phi_i^T) \tag{4b}$$

$$k_n/k_0 = (\text{KIE})^{-n} \tag{4c}$$

In these equations, k_n is the rate constant in n mole fraction of D_2O, k_0 is the rate constant in H_2O, x is the number of exchangeable sites in the transition state experiencing changes in fractionation factor(s), and ϕ^T, known as the fractionation factor, is the transition state isotope exchange equilibrium constant. Whereas eq 4a assumes equal contributions from the x sites, therefore giving a ϕ^T value that does not change when multiple sites fractionate ($x > 1$), eq 4b, describing the more general case, does not make such an assumption, giving disparate ϕ_i^T values when multiple sites are involved; in either case, the product $(\phi^T)^i$ or $(\phi_i^T)^i$ would equal the inverse of the isotope effect (k_{DOD}/k_{HOH}). Equation 4c describes a medium effect where the parameter determined from the fit is the KIE itself, k_{HOH}/k_{DOD} (*10*).

The pL (L = H, D) dependence of rate constant k_4 was fit to eq 5, which models an apparent single ionization, where Y represents the values of the measured rate constant, K_a the equilibrium constant linking the two binding states, k_{AH} the value of the rate constant at low pH (protonated form), and k_{A-} the value of the same rate constant at high pH (unprotonated form) (*11*).

$$Y = \frac{k_{AH}[H^+] + K_a k_{A-}}{[H^+] + K_a} \tag{5}$$

Steady-state rate equations based on the rate constants observed for the steps depicted in Scheme 2 are shown in eqs 6 and 7. Derivation was by the net rate constant method.

$$k_{cat} = \frac{1}{\frac{k_1[O_2] + k_{off}}{k_{on}[HPP]k_1[O_2]} + \frac{1}{k_1[O_2]} + \frac{1}{k_2} + \frac{1}{k_3} + \frac{1}{k_4}} \tag{6}$$

$$\frac{k_{cat}}{K_{HPP}} = \frac{k_{on}k_1[O_2]}{k_1[O_2] + k_{off}} \tag{7}$$

RESULTS AND DISCUSSION

HMS, along with HPPD, catalyzes the oxidative decarboxylation and subsequent oxygenation of a single molecule. In all

Table 1: Steady-State Kinetic Parameters[a] for HMS

substrate/solvent or effect	k_{cat} (s^{-1})	K_{mHPP} (μM)	k_{cat}/K_{mHPP} (mM^{-1} s^{-1})	K_{mO_2} (μM)[b]	k_{cat}/K_{mO_2} (mM^{-1} s^{-1})
3′,3′-diprotio/H_2O	0.23 ± 0.01	6.5 ± 0.8	36 ± 4	9 ± 4	26 ± 12
3′,3′-dideuterio/H_2O	0.22 ± 0.01	7.1 ± 1.4	31 ± 5		
substrate KIE	1.04 ± 0.06		1.16 ± 0.27		
3′,3′-diprotio/D_2O	0.072 ± 0.002	1.9 ± 0.3	38 ± 5		
solvent KIE	3.3 ± 0.2		0.95 ± 0.16		

[a]All values measured at 5 °C in the presence of 2.1 μM HMS, 20 μM ferrous sulfate heptahydrate, 500 μM dithioreitol, and 20 mM HEPES, pH 7.0. [b]The value for K_{mO_2} was underdetermined and approximate.

there are four activities known for these two enzymes. HMS accepts both HPP and phenylpyruvate as substrates, and mammalian HPPDs use HPP and α-ketoisocaproate as substrates (*12*). While these enzymes are members of the α-keto acid-dependent oxygenase (αKAO) superfamily (*13*), none of them uses the α-keto acid, α-ketoglutarate, that all other members use. Instead, they derive the reducing equivalents required to activate molecular oxygen from an α-keto acid moiety on the molecule they ultimately hydroxylate. Of the activities in this subclass, HPPD reacting with HPP is the most studied due to its intriguing chemical conversion and the relevance of its inhibition to agrochemistry and specific rare inherited diseases (*4*). HMS uses the same substrates as HPPD, HPP, and dioxygen but manages to avoid hydroxylation of the activated aromatic ring and hydroxylates the relatively inert adjacent benzylic carbon. Despite the homology and structural similarity shared by HPPD and HMS, each enzymatic reaction has complete hydroxylation regiospecificity (*3*, *7*, *14*).

Compared to HPPD, HMS is a relatively recent discovery, and this is the first study to characterize its kinetic properties (*3*, *5*, *6*). We present and discuss below measurements of steady-state parameters, substrate binding, and rate constants for individual catalytic steps measured in single turnover reactions under a variety of conditions. The spectrum of a rapidly accumulating and decaying intermediate that absorbs most strongly at low wavelengths is revealed through global deconvolution of PDA data. Although this species accumulates early and to very low levels, its existence can be established by comparison of the relative starting and end absorbance values for traces observed at different wavelengths. The third process exhibits no kinetic isotope effect in the presence of 2,2′-dideuterio-HPP despite the fact that the product, HMA, can be shown to be formed in this step, and the rate-limiting fourth phase is identified, as product release, and is assisted by the movement of a single solvent-derived proton.

Steady-State Kinetic Data. Steady-state kinetic parameters were measured at 5 °C such that they could be compared directly to transient state kinetic observations. The release of Fe(II) from the enzyme was measured under anaerobic conditions using the Fe(II)-specific chelator, Ferene S, according to the methods of Johnson Winters et al. (*7*). The observed k_{off} for Fe(II) was ~0.00035 ± 0.00001 s^{-1} (data not shown). This value indicates that it is valid to assume that the release of Fe(II) by the enzyme need not be taken into consideration in the time frame of typical assays used for steady-state analyses and that concentrations of iron equal to that of the enzyme are sufficient to fully occupy the available active sites.

The K_m for molecular oxygen could not be accurately determined but was estimated to be quite low (~5−15 μM). For this reason, apparent steady-state kinetic parameters for HMS in turnover with HPP were measured at an O_2 concentration that corresponded to the zero-order segment of the O_2 Michaelis curve (~400 μM). These data indicate that HMS has a turnover number (k_{cat}) of 0.23 ± 0.01 s^{-1} and a K_{mHPP} of 6.5 ± 0.8 μM. In the presence of 3′,3′-dideuterio-HPP, neither k_{cat} nor K_{mHPP} changed significantly. In D_2O, the k_{cat} decreased by more than 3-fold but was accompanied by a corresponding decrease in K_{mHPP} of 3.5-fold, leaving the apparent k_{cat}/K_{mHPP} ostensibly unchanged (Table 1). This decrease in the K_{mHPP} value is consistent with the transient state kinetic observations and is discussed further below.

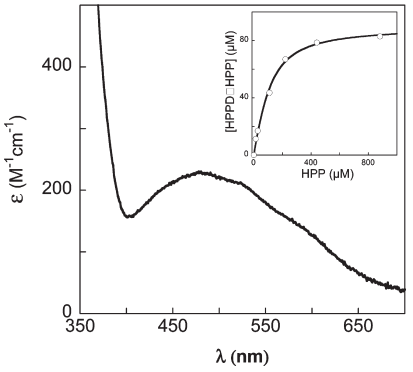

FIGURE 1: The charge-transfer absorbance spectrum of the HMS·Fe(II)·HPP complex under anaerobic conditions. Inset: Binding isotherm at 4 °C for HPP (○) titrated against 99 μM HMS in the presence of 96 μM Fe(II) (i.e., 96 μM HMS·Fe(II) complex) in 20 mM HEPES, pH 7.0. The data were fit to eq 2.

Binding of HPP to HMS. Bidentate association of α-keto acids with a coordinated ferrous ion gives rise to metal-to-ligand charge-transfer absorption bands (*15*−*17*). Under anaerobic conditions these can be used as a signal to generate binding isotherms to obtain the fractional saturation of an enzyme sample in the presence of a known concentration of ligand (*18*). The titration of HPP to HMS induced a charge-transfer band very similar to that observed with HPPD and other αKAO enzymes (λ_{max} = 475 nm, ε_{475} = 250 M^{-1} cm^{-1}) (*7*, *15*−*20*). The development of the charge-transfer absorption band was rapid, and the system was at equilibrium within the time taken to fully mix the enzyme and substrate (~10 ms). This suggests that association and dissociation of HPP to and from the holoenzyme are fast. The dissociation constant for the substrate was determined to be 59 ± 8 μM (Figure 1). The fit of the data determined that 92% of the enzyme was available to bind the substrate.

Product Analysis of HPP. In order to test the regiospecificity of the hydroxylation reaction, product analyses of multiple turnover reactions were conducted using HPLC. HMS and HPPD are mechanistic homologues, and delivery of the second oxygen atom dictates the product formed in each case (Scheme 1). If the HPP conformation within the two enzymes were similar, these two positions of oxygenation are ~1.5 Å apart, and some

amount of the alternate product may reasonably be expected to form from either enzyme. With a limit of detection for HG of 27 pmol and assuming that the k_{cat} values for the formation of HMA and HG from HMS are similar, we can conclude that the HMS reaction has at least 99.5% fidelity. This strongly suggests that the conformation and/or orientation of the substrate and subsequent intermediates differ(s) sufficiently from those of HPPD such that aromatic hydroxylation is made considerably less likely in HMS, a notion recently put forward by Neidig et al. (*21*) and addressed more fully by Brownlee et al. (*3*).

Oxidation of the Holoenzyme. The HMS holoenzyme reacts with dioxygen in the absence of the substrate, HPP, to yield the ferric form of the enzyme. This oxidation can be observed as an increase in absorbance in the 300−340 nm region of the spectrum. The observed rate constant for oxidation shows a linear dependence on O_2 concentration, with a zero *y*-intercept. The reaction is thus bimolecular irreversible and has a second-order rate constant of 34.7 ± 0.8 M^{-1} s^{-1} (Figure 2). If the enzyme were to reduce O_2 prior to binding HPP, this value indicates that assuming an O_2 concentration of 390 μM at 5 °C the maximum rate of turnover possible under these conditions is 0.013 s^{-1}, ~20-fold slower than the observed k_{cat} (see above). This result supports the conclusion that HPP adds to the enzyme first in normal catalysis. This result is confirmatory, as HPPD exhibits a nearly identical holoenzyme oxidation rate for the free enzyme, and a change in the order of substrate addition in HMS relative to HPPD was not expected. Moreover, the order of addition for other α-keto acid-dependent enzymes also has O_2 adding after all other substrates are bound (*22*). It is known that in the HMS·Fe(II)·HPP complex the α-keto acid is made planar and as such is conjugated with the metal ion (*21*). This conjugation increases the electron density at the metal and promotes the reduction of dioxygen during collision. The changing reactivity of the metal ion toward dioxygen in the presence and absence of HPP is the basis for the defined order of addition of the two substrates.

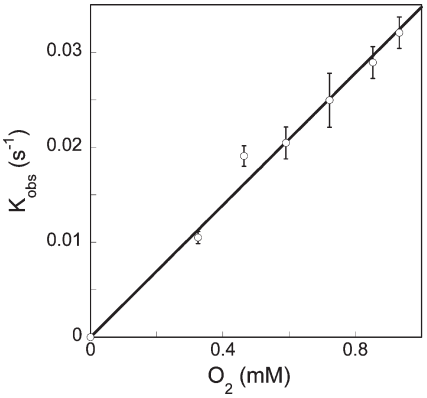

FIGURE 2: The oxidation of the HMS·Fe(II) complex in the presence of dioxygen monitored at 310 nm. Varied oxygen concentrations were mixed with anaerobic holoenzyme (12.5 μM HMS, 10 μM Fe(II) final) at 4 °C.

Single Turnover Reactions. In single turnover reactions the HMS·Fe(II)·HPP complex was mixed with dioxygen, and observations were made with either a photomultiplier (PMT) or photodiode array (PDA). In PMT mode, the wavelength of observation was most often at the substrate complex charge transfer maximum at 445 or 450 nm. Experiments were conducted under a variety of conditions: at different dioxygen concentrations, using protiated or dideuterated substrate, in H_2O or D_2O, and at different pHs. Experiments were first conducted under pseudo-first-order conditions to preliminarily define rate constants, as the number of models that pseudo-first-order traces can fit to is generally smaller. A trace collected at 445 nm for a reaction pseudo-first-order in enzyme is displayed in Figure 3.

Unlike the related HPPD system, mixing is associated with considerable Schlierin artifacts for the HMS system. Despite the dead time for the stopped-flow instrument being ~1.6 ms, data collected prior to about 10 ms were obscured by this phenomenon (Figure 3B). In order to lessen this complication, the majority of the single turnover experiments were conducted with the enzyme complex and the O_2 concentrations being matched or similar. This approach has the added advantage of using lower concentrations of enzyme and higher concentrations of O_2, thereby increasing the signal-to-noise ratio compared to pseudo-first-order experiments. Qualitatively, traces from such experiments were a decrease followed by an increase, which can most clearly be observed in the multiwavelength-time landscape formed by PDA data sets (Figures 4A and 4B).

Ultimately the minimal four-phase model depicted in Scheme 2 was used to fit all data sets to a consistent set of rate constants for all experimental conditions. However, the rate constants for the first two events were not measured, as the first event is almost completely obscured by the mixing artifact and the second phase is rapid. Respectively, these two limitations obscure and diminish the accumulation of the first intermediate. A fit depicting the application of this model is shown in Figure 3B. The imposition of this model is required by the wavelength dependence of the

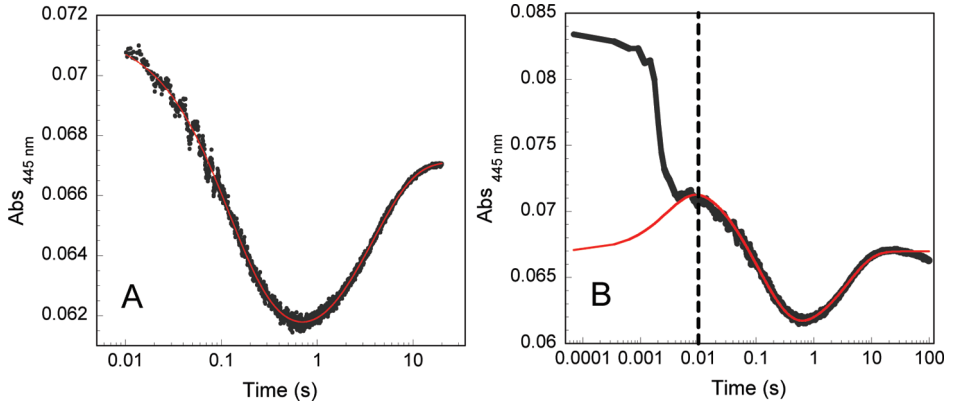

FIGURE 3: Pseudo-first-order reaction of 190 μM HMS·Fe(II)·HPP and 19.8 μM O_2 monitored at 445 nm. (A) The 0.01−20 s portion with fit (red). (B) The entire data set collected for this reaction with the fit extrapolated to time points prior to 0.01 s, indicated by the dashed vertical line, to illustrate how data at early time points were obscured by mixing artifacts.

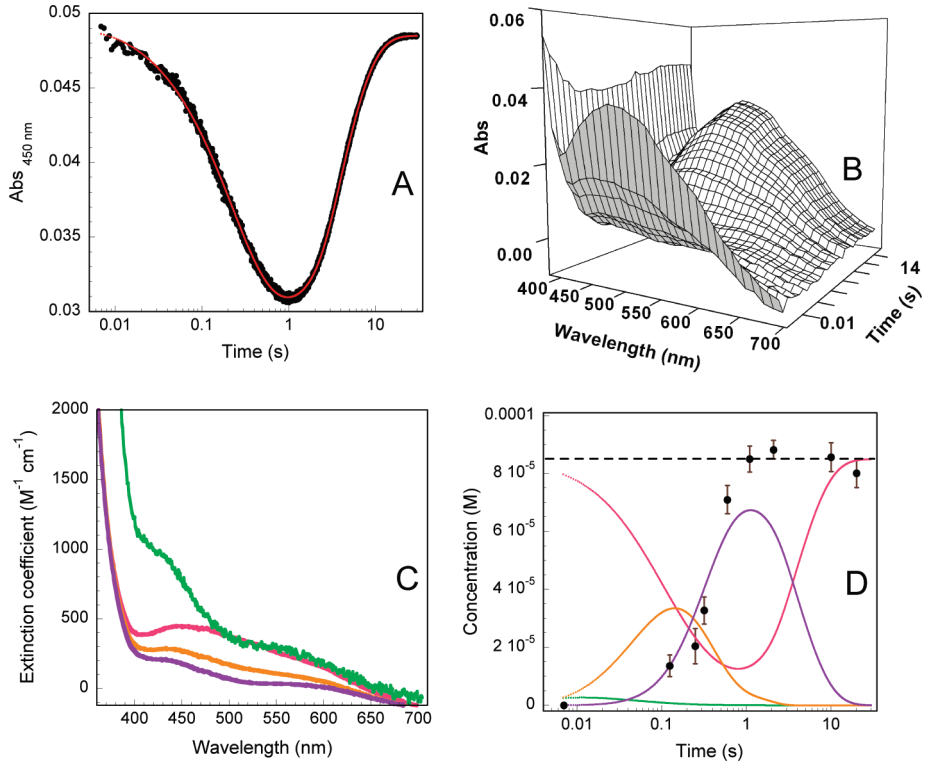

FIGURE 4: Single turnover reactions of the HPP-bound HMS holoenzyme and O_2. (A) 85 μM HMS·Fe(II)·HPP reacting with 80 μM O_2 at 450 nm; data in dark gray and fit in red. (B) Multiwavelength−time landscape formed from PDA data sets of 150 μM HMS·Fe(II)·HPP reacting with 150 μM O_2. (C) Deconvoluted spectra of all species observed from the reaction of (A) observed in PDA mode and fit to $k_1 = 1 \times 10^5\ M^{-1}\ s^{-1}$, $k_2 = 250\ s^{-1}$, $k_3 = 5\ s^{-1}$, and $k_4 = 0.3\ s^{-1}$. The initial HMS·Fe(II)·HPP charge transfer and intermediates I, II, and III are respectively represented in pink, green, orange, and violet. (D) Simulated accumulation profiles of all four species using the same set of four rate constants and shown in the same color scheme as in (C) overlaid with rapid-quench product analysis for HMA. The dashed line indicates the concentration of enzyme.

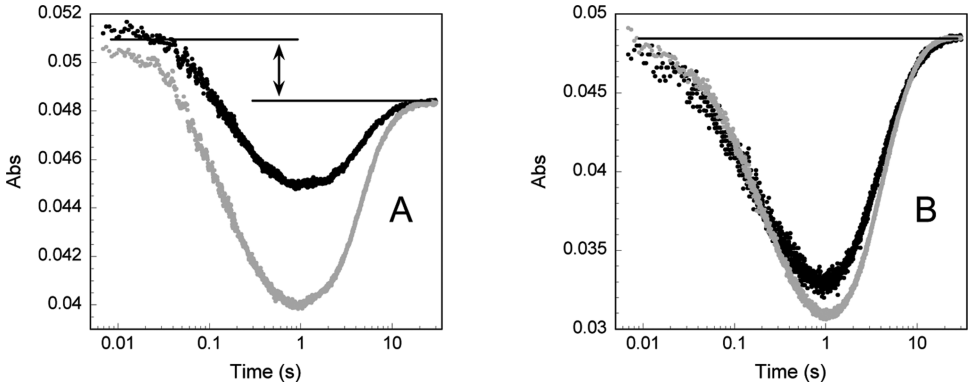

FIGURE 5: 85 μM HMS·Fe(II)·HPP reacting with 80 μM O_2 in H_2O monitored at various wavelengths. (A) The 399 and 375 nm traces (gray and black, respectively). (B) Reactions monitored at 450 and 550 nm (gray and black, respectively).

relative start and end points in single wavelength traces. Experimental design was such that all dioxygen was consumed in the reaction and the substrate complex is re-formed once the product is released (Scheme 2). If the spectrum of HMS's intermediate I is indeed as that shown in Figure 4C, time-dependent absorption data at wavelengths lower than 450 nm should display noticeably higher absorbance at 10 ms relative to the end point. This pattern is borne out by the PMT traces shown in Figure 5A, collected at 399 and 375 nm for the same reaction, whereas traces collected at longer wavelengths do not have this characteristic (Figure 5B). Elevated absorbances at early times with respect to the end point absorbance values suggest that we have largely failed to observe an intermediate(s) prior to the end of the mixing and must include the formation and decay of this intermediate in our kinetic model.

Despite the paucity of evidence, the shape of the spectrum of the first intermediate species can be deconvoluted from the PDA data when fit to the model depicted in Scheme 2. However, the lack of data at early times requires that we impose a value for k_1 that in turn defines the extinction coefficients depicted for this species. As such, the true absorbency of this species cannot be deduced from the available data. Figure 4C depicts the calculated intermediate spectrum for this species, assuming a value for k_1 ($10^5\ M^{-1}s^{-1}$) that is on the same order of magnitude as that observed for the closely related HPPD enzyme ($7.4 \times 10^4\ M^{-1}\ s^{-1}$) (*9*), and the shape of this species is qualitatively similar to the first intermediate observed in single turnover reactions of HPPD (*9*, *23*).

The range of rate constant values observed for k_2 from fitting was broad. What was clear was that the second phase was relatively rapid and largely responsible for the low fractional

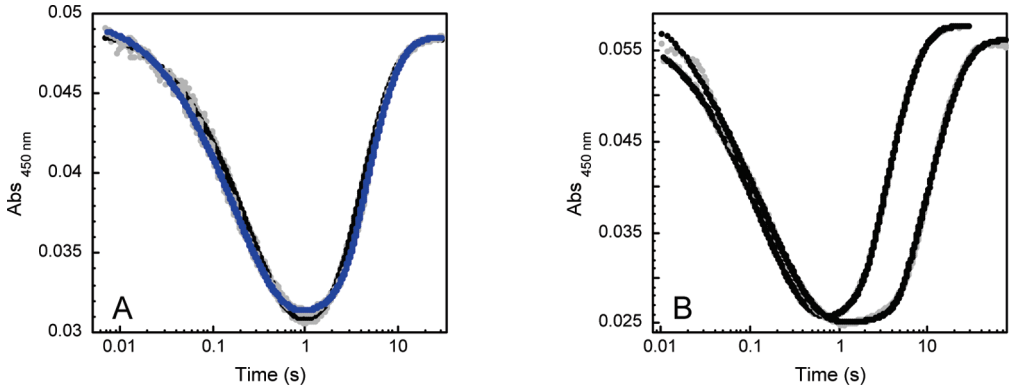

FIGURE 6: Single turnover reactions with dideuterio-HPP and in D_2O solvent. (A) Overlaid traces of 85 μM HMS·Fe(II)·HPP and 85 μM HMS·Fe(II)·dideuterio-HPP reacting with 80 μM O_2 in H_2O, monitored at 450 nm. Data are in gray for both, while the fit is in black for HPP and in blue for dideuterio-HPP. (B) Overlaid traces of 150 μM HMS·Fe(II)·HPP reacting with 145 μM O_2 in H_2O versus D_2O, monitored at 450 nm; data in gray and fit in black.

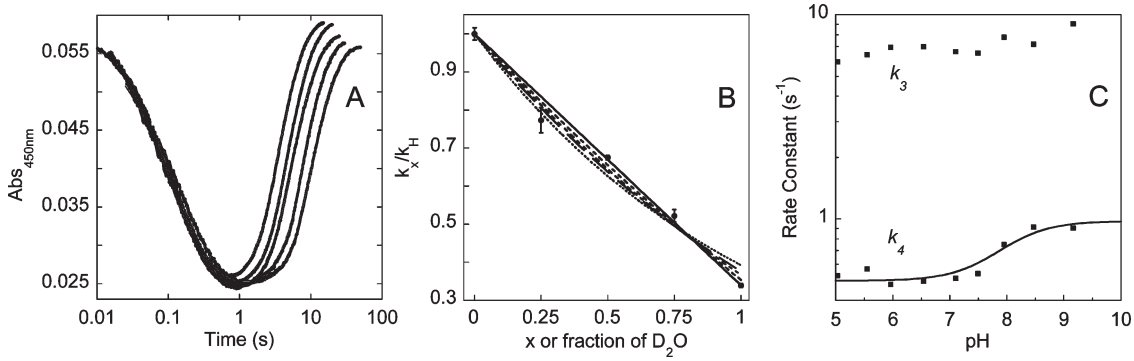

FIGURE 7: Effect of exchanging solvent to D_2O and varying pH on the HMS single turnover reaction rates. (A) Five 450 nm traces of 150 μM HMS·Fe(II)·HPP reacting with 145 μM O_2 in 0%, 25%, 50%, 75%, and 100% D_2O solvent. For each trace, data are depicted with black lines and the fit for each trace is in gray. (B) Dependence of the ratio of the rate constants in H_2O and in various fractions of D_2O for the last, limiting process on the fraction of D_2O. Fits are to eqs 4a and 4c that assume equal contribution from each site of exchange in the transition state and are for one, two, three, and many sites (solid, small dashed, dashed, and dotted lines, respectively). (C) pH dependence of the rate constants of the last two processes in the single turnover reactions. The line overlaying the k_4 data points is this curve's fit to eq 5, resulting in a pK_a of 8.0.

accumulation of the first intermediate (~5%), which greatly hampered the accurate measurement of this rate constant. Due to the dearth of information required to accurately define the first two rate constants, k_2 was also modeled at a fixed value (250 s^{-1}) that, while quite uninformative, gave consistently good fits for all data sets. As may be seen in the quality of fits in Figures 4A, 6A, and 7A, these values do provide a very good description of the absorbance changes observed. The set of four rate constants that recreates well the trace of a typical reaction is k_1 = 1×10^5 M^{-1} s^{-1}, k_2 = 250 s^{-1}, k_3 = 5 s^{-1}, and k_4 = 0.3 s^{-1}.

HPPD's smaller k_2 value of 74 s^{-1}, by contrast, provided both later and significantly greater accumulation of HPPD's first intermediate. This together with its better mixing properties meant that single turnover data collection for HPPD missed only 40% of the accumulation of the first transient (*9*).

Chemical Quench and Product Analysis. The HMS reaction was quenched at multiple time points from 100 ms to 20 s and analyzed for HMA. The results are shown in Figure 4D, superimposed on the accumulation profile. HMA production tracks well with the accumulation of intermediate III and plateaus at the stoichiometric 100% product level (indicated by the dashed line) around 1 s. These data strongly support that intermediate III is the product complex (HMS·Fe(II)·HMA) and that the most natural interpretation of the final phase is hydroxymandelate release given that the HMS·Fe(II)·HPP complex charge transfer is re-formed in this phase.

Table 2: Pre-Steady-State Rate Constants for HMS

expt no.	substrate/solvent	k_1[a] (M^{-1} s^{-1})	k_2[b] (s^{-1})	k_3 (s^{-1})	k_4 (s^{-1})
1	3′,3′-diprotio/H_2O	1×10^5	250	4.8 ± 0.1	0.28 ± 0.01
2	3′,3′-dideuterio/H_2O	1×10^5	250	6.2 ± 0.1	0.28 ± 0.02
5	3′,3′-diprotio/D_2O	1×10^5	250	5.3 ± 0.4	0.10 ± 0.01
					solvent KIE 2.8

[a]Not a measured value but rather an estimate of the rate constant based on the value measured in related enzymes. [b]Underdetermined value from fitting. The low fractional accumulation of the first intermediate undermines accurate measurement of the value for this rate constant. The rate constant used provides consistently good fits for all data sets but is not directly informative.

Calculated Steady-State Parameters. Based on eq 6 and Scheme 2 and using the pre-steady-state rate constants derived from fitting in Table 2, the steady-state parameter k_{cat} was calculated. In these calculations, k_{on} for HPP was assumed to be at the diffusion limit (10^9 M^{-1} s^{-1}), which gives a k_{off} of 5.9 × 10^4 s^{-1}, based on the experimentally determined K_{dHPP} of 59 μM. Steady-state assays were carried out with an enzyme concentration of 2.1 μM and with 90% saturation by HPP (430 μM), and an O_2 concentration of ~390 μM. Based on these parameters, substitution into eqs 6 for the diprotio/H_2O, dideuterio/H_2O, and diprotio/D_2O cases gave k_{cat} values of 0.26, 0.27, and 0.08 s^{-1}, respectively. These calculated values are all in good agreement

Scheme 3: Proposed Mechanism for HMS

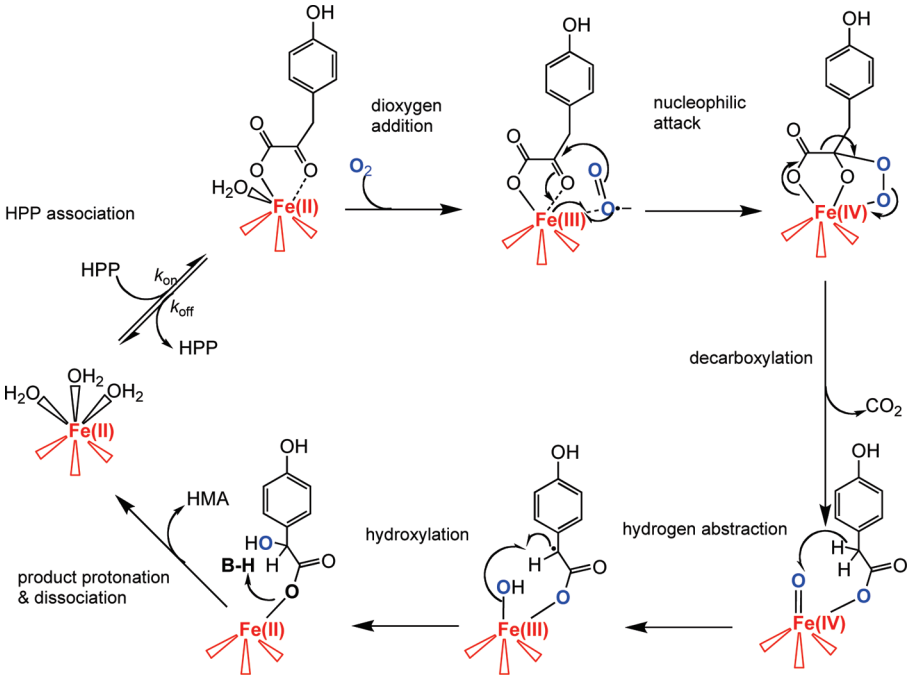

with the experimental steady-state values in Table 2. The value of k_{cat}/K_{mHPP} is thought to provide an approximation of the second-order rate constant for the addition of HPP to the enzyme. As such, it would not be predicted to change in response to deuterated solvent if the only step affected were the final and primarily rate-limiting HMA release step (k_4). This is consistent with eq 7, the expression for k_{cat}/K_{mHPP}, that does not include the k_4 term. Rearranging eq 7 for K_{mHPP}, we see that the observed 3.5-fold decrease in the measured K_{mHPP} value in D_2O occurs due to the k_{cat} term residing in the numerator of the K_{mHPP} expression. Since k_{cat} is dominated by k_4, changes in the value of this rate constant will be observed in the value of K_{mHPP}.

Effects of Deuterated Substrate. Traces collected at 450 nm from single turnover experiments using HPP and 3′,3′-dideuterio-HPP appear in Figure 6A. The rate constants derived from fitting these traces are summarized in Table 2; however, the major conclusion is evident from observing the superimposed traces themselves: no primary substrate kinetic isotope effect is observed despite the fact that breaking the bond between the benzylic carbon and one of its hydrogens is necessary for hydroxylation. Consistent with earlier mechanistic conclusions, hydroxylation could most likely be brought about by an electrophilic attack from an iron(IV)−oxo species, and the substitution of a deuteron to the carbon ultimately hydroxylated has been a viable strategy to prolong the life of the hydroxylating species in other related systems (*24*−*27*). For HMS, no significant difference in any of the rate constants was observed upon substitution of deuterons at that benzylic position of HPP. This suggests that the expected H-atom abstraction is fast relative to preceding and subsequent events and is not observed in the single turnover reactions.

Solvent KIE on k_4, Proton Inventory, and pH Dependence. k_4 is strongly supported by chemical quench to be the HMA release step. Because k_4 is rate-limiting, the observed solvent KIE of 3 on this step is quite consistent with the solvent KIE of 3.3 observed for the steady-state k_{cat} value. This value is comparable to the solvent KIE observed for the decay of the product complex and re-formation of the charge transfer in the closely related HPPD enzyme, verified in that system not only by chemical quench but also by fluorescence stopped flow (*9*). This resemblance to the related enzyme bolsters the conclusion that the fourth phase for HMS is hydroxymandelate release and that intermediate III is indeed the product complex.

A solvent KIE indicates that solvent-derived protons are in flight during the last phase. In order to ascertain the number of protons in flight, a proton inventory was conducted. Traces from reactions comprising the inventory, carried out in solvents with five different D_2O fractions, are shown in Figure 7A, and the D_2O fraction dependence is plotted in Figure 7B. In Figure 7B, fits for one, two, and three fractionating sites are shown assuming equal-site contribution and using eq 4a to give ϕ^T values of 0.34 ± 0.02, 0.61 ± 0.02, and 0.72 ± 0.01, respectively. The fourth fit is for the so-called medium effect, where the parameter fit for k_{HOH}/k_{DOD} is the KIE itself and is 2.55 ± 0.15. Although standard errors for the first three cases are comparable, visual inspection indicates that the single-site case approximates the actual dependence best, with the line of fit passing straight through the 0%, 50%, and 100% D_2O data points and touching the 75% point. The 25% D_2O point exhibits the largest deviation from this model and is likely an outlier.

In theory, fractionation factors are equivalent to individual *inverted* isotope effect values from the sites that fractionate and, therefore, when multiplied together in each case should give the reciprocal of the isotope effect; here k_{HOH}/k_{DOD} = 0.29 (*28*). That the value of 0.34 ± 0.02 from the single-site fit agrees best with 0.29 supports the conclusion that only a single site is involved. For the two-site case, a fit using the more general model of eq 4b that does not make the equal-site contribution assumption was also made, resulting in disparate fractionation factor values: ϕ_1^T = 0.41 ± 0.14 and ϕ_2^T = 0.85 ± 0.24, with noticeably larger errors than the results from the equal-site contribution fits. Thus, the general conclusion is that the surroundings contribute a single proton that participates in the transition state for this step. While definitive identification of the

proton involved in the solvent KIE is difficult to make, in the case under discussion, the proton donor may be a water molecule buried in the active site and adjacent to the carboxylate of the product that was observed in the recently solved X-ray structure of the HMS·Fe(II)·HMA complex (*3*).

The solvent KIE suggests that product protonation accompanies its dissociation (as depicted in Scheme 3). HMA's two carboxylate oxygen atoms, observed in the X-ray structure to be 3.82 and 1.69 Å away from the metal center, are the only open valences on the product able to accept a proton. A well-defined water molecule only 3.45 Å from the distal oxygen atom may well fulfill the role of the proton donor and assist in HMA's dissociation. This water molecule has four potential H-bonding interactions to three universally conserved residues, which contribute two main chain amide groups that may help to stabilize a hydroxide anion after deprotonation (*3*). Further, the water molecule is located at the crucial hinge region of the C-terminal helix that has been observed to adopt multiple conformations in HPPD structures, suggesting that movement of this helix could be coupled with product release (*29*−*32*).

Solvent pL (L = H, D) in the proton inventory experiments was maintained at 7.0. A pH study was carried out to be assured that rate constants in the inventory were measured at a position where, most particularly for k_4, $dk/dpL \approx 0$ such that the effects observed in the inventory were intrinsic to the system and not due to perturbations in pL. This study revealed that k_4 increases by nearly an order of magnitude at high pH but that there was a relatively flat pH dependence for both k_3 and k_4 in the region spanning ±0.5 unit of pH 7.0 (Figure 7C). A pD dependence study was therefore unnecessary, as the typical greatest difference in buffer pK_a values in D_2O compared to H_2O is less than 0.5 pH unit (*33*). k_4's pH dependence is best characterized by a single ionization event despite some variability in the low-pH data points, giving a pK_a of 8.0 ± 0.2 when fit to eq 5 (Figure 7C). This pK_a is consistent with a basic residue acting as a catalyst to assist with deprotonation and would be low for a water molecule but not inconceivable given the contact environment.

The proposed mechanism in Scheme 3 is based on the consensus mechanism of decarboxylation and aliphatic hydroxylation that is possibly the most common chemistry observed in the α-keto acid dependent oxygenases. Our results indicate that benzylic oxygenation in HMS is rapid relative to the other observed steps and unable to be probed by deuterium substitution. Although more definitive evidence regarding early parts of the scheme would have been welcome, our evidence support the following: that a fast-disappearing early intermediate exists that absorbs relatively more strongly below 450 nm, that hydrogen atom abstraction is neither rate-limiting nor is it the step observed prior to HMA formation, that the final intermediate is the product complex, and that the decay of this species is rate limiting in turnover.

ACKNOWLEDGMENT

We express our sincere thanks to Professor Christopher T. Walsh from the Department of Biological Chemistry and Molecular Pharmacology at Harvard Medical School for willingly supplying the gene for HMS. We also express our thanks to our colleague Holger Fosterling of the Department of Chemistry and Biochemistry at the University of Wisconsin—Milwaukee for assistance in the collection and compilation of nuclear magnetic resonance data associated with exchange of benzylic protons in deuterated solvents.

REFERENCES

1. Walsh, C. (2000) Molecular mechanisms that confer antibacterial drug resistance. *Nature 406*, 775–781.
2. Li, L., and Xu, B. (2005) Multivalent vancomycins and related antibiotics against infectious diseases. *Curr. Pharm. Des. 11*, 3111–3124.
3. Brownlee, J., He, P., Moran, G. R., and Harrison, D. H. (2008) Two roads diverged: the structure of hydroxymandelate synthase from *Amycolatopsis orientalis* in complex with 4-hydroxymandelate. *Biochemistry 47*, 2002–2013.
4. Moran, G. R. (2005) 4-Hydroxyphenylpyruvate dioxygenase. *Arch. Biochem. Biophys. 433*, 117–128.
5. Hubbard, B. K., Thomas, M. G., and Walsh, C. T. (2000) Biosynthesis of L-p-hydroxyphenylglycine, a non-proteinogenic amino acid constituent of peptide antibiotics. *Chem. Biol. 7*, 931–942.
6. Choroba, O. W., Williams, D. H., and Spencer, J. B. (2000) Biosynthesis of the vancomycin group of antibiotics: involvement of an unusual dioxygenase in the pathway to (S)-4-hydroxyphenylglycine. *J. Am. Chem. Soc. 122*, 5389–5390.
7. Johnson-Winters, K., Purpero, V. M., Kavana, M., Nelson, T., and Moran, G. R. (2003) 4-(Hydroxyphenyl)pyruvate dioxygenase from *Streptomyces avermitilis*: the basis for ordered substrate addition. *Biochemistry 42*, 2072–2080.
8. Pace, N. C., Vajdos, F., Fee, L., Grimsley, G., and Gray, T. (1995) How to measure and predict the molar absorption coefficient of a protein. *Protein Sci. 4*, 2411–2423.
9. Johnson-Winters, K., Purpero, V. M., Kavana, M., and Moran, G. R. (2005) Accumulation of multiple intermediates in the catalytic cycle of (4-hydroxyphenyl)pyruvate dioxygenase from *Streptomyces avermitilis*. *Biochemistry 44*, 7189–7199.
10. Quinn, D. M. (2006) Theory and practice of solvent isotope effects, in Isotope Effects in Chemistry and Biology (Kohen, A., and Limbach, H.-H., Eds.) pp 995−1018, CRC Press, Taylor & Francis Group, Boca Raton, FL.
11. Harris, C. M., Pollegioni, L., and Ghisla, S. (2001) pH and kinetic isotope effects in D-amino acid oxidase catalysis. *Eur. J. Biochem. 268*, 5504–5520.
12. Baldwin, J. E., Crouch, N. P., Fujishima, Y., Lee, M. H., MacKinnon, C. H., Pitt, J. P. N., and Willis, A. C. (1995) 4-Hydroxyphenylpyruvate dioxygenase appears to display alpha-ketoisocaproate dioxygenase activity in rat liver. *Bioorg. Med. Chem. Lett. 5*, 1255–1260.
13. Hausinger, R. P. (2004) FeII/alpha-ketoglutarate-dependent hydroxylases and related enzymes. *Crit. Rev. Biochem. Mol. Biol. 39*, 21–68.
14. Gunsior, M., Ravel, J., Challis, G. L., and Townsend, C. A. (2004) Engineering p-hydroxyphenylpyruvate dioxygenase to a p-hydroxymandelate synthase and evidence for the proposed benzene oxide intermediate in homogentisate formation. *Biochemistry 43*, 663–674.
15. Pavel, E. G., Zhou, J., Busby, R. W., Gunsior, M., Townsend, C. A., and Solomon, E. I. (1998) Circular dichroism and magnetic circular dichroism spectroscopic studies of the non-heme ferrous active site in clavaminate synthase and its interaction with alpha-ketoglutarate cosubstrate. *J. Am. Chem. Soc. 120*, 743–753.
16. Neidig, M. L., Kavana, M., Moran, G. R., and Solomon, E. I. (2004) CD and MCD studies of the non-heme ferrous active site in (4-hydroxyphenyl)pyruvate dioxygenase: correlation between oxygen activation in the extradiol and alpha-KG dependent dioxygenases. *J. Am. Chem. Soc. 126*, 4486–4487.
17. Neidig, M. L., Decker, A., Kavana, M., Moran, G. R., and Solomon, E. I. (2005) Spectroscopic and computational studies of NTBC bound to the non-heme iron enzyme (4-hydroxyphenyl)pyruvate dioxygenase: active site contributions to drug inhibition. *Biochem. Biophys. Res. Commun. 338*, 206–214.
18. Ryle, M. J., Padmakumar, R., and Hausinger, R. P. (1999) Stopped-flow kinetic analysis of *Escherichia coli* taurine/alpha- ketoglutarate dioxygenase: interactions with alpha-ketoglutarate, taurine, and oxygen. *Biochemistry 38*, 15278–15286.
19. Grzyska, P. K., Ryle, M. J., Monterosso, G. R., Liu, J., Ballou, D. P., and Hausinger, R. P. (2005) Steady-state and transient kinetic analyses of taurine/alpha-ketoglutarate dioxygenase: effects of oxygen concentration, alternative sulfonates, and active-site variants on the FeIV-oxo intermediate. *Biochemistry 44*, 3845–3855.
20. Ho, R. Y., Mehn, M. P., Hegg, E. L., Liu, A., Ryle, M. J., Hausinger, R. P., and Que, L., Jr. (2001) Resonance Raman studies of the iron(II)-alpha-keto acid chromophore in model and enzyme complexes. *J. Am. Chem. Soc. 123*, 5022–5029.

21. Neidig, M. L., Decker, A., Choroba, O. W., Huang, F., Kavana, M., Moran, G. R., Spencer, J. B., and Solomon, E. I. (2006) Spectroscopic and electronic structure studies of aromatic electrophilic attack and hydrogen-atom abstraction by non-heme iron enzymes. *Proc. Natl. Acad. Sci. U.S.A. 103*, 12966–12973.
22. Purpero, V., and Moran, G. R. (2007) The diverse and pervasive chemistries of the alpha-keto acid dependent enzymes. *J. Biol. Inorg. Chem. 12*, 587–601.
23. Purpero, V. M., and Moran, G. R. (2006) Catalytic, noncatalytic, and inhibitory phenomena: kinetic analysis of (4-hydroxyphenyl)-pyruvate dioxygenase from *Arabidopsis thaliana*. *Biochemistry 45*, 6044–6055.
24. Price, J. C., Barr, E. W., Glass, T. E., Krebs, C., and Bollinger, J. M., Jr. (2003) Evidence for hydrogen abstraction from C1 of taurine by the high-spin Fe(IV) intermediate detected during oxygen activation by taurine:alpha-ketoglutarate dioxygenase (TauD). *J. Am. Chem. Soc. 125*, 13008–13009.
25. Price, J. C., Barr, E. W., Tirupati, B., Bollinger, J. M., Jr., and Krebs, C. (2003) The first direct characterization of a high-valent iron intermediate in the reaction of an alpha-ketoglutarate-dependent dioxygenase: a high-spin FeIV complex in taurine/alpha-ketoglutarate dioxygenase (TauD) from *Escherichia coli*. *Biochemistry 42*, 7497–7508.
26. Hoffart, L. M., Barr, E. W., Guyer, R. B., Bollinger, J. M., Jr., and Krebs, C. (2006) Direct spectroscopic detection of a C-H-cleaving high-spin Fe(IV) complex in a prolyl-4-hydroxylase. *Proc. Natl. Acad. Sci. U.S.A. 103*, 14738–14743.
27. Galonic, D. P., Barr, E. W., Walsh, C. T., Bollinger, J. M., Jr., and Krebs, C. (2007) Two interconverting Fe(IV) intermediates in aliphatic chlorination by the halogenase CytC3. *Nat. Chem. Biol. 3*, 113–116.
28. Schowen, R. L. (2006) Hydrogen bonds, transition state stabilization, and enzyme catalysis, in Istope Effects in Chemistry and Biology (Kohen, A., and Limbach, H.-H., Eds.) pp 765−792, CRC Press, Taylor & Francis Group, Boca Raton, FL.
29. Serre, L., Sailland, A., Sy, D., Boudec, P., Rolland, A., Pebay-Peyroula, E., and Cohen-Addad, C. (1999) Crystal structure of *Pseudomonas fluorescens* 4-hydroxyphenylpyruvate dioxygenase: an enzyme involved in the tyrosine degradation pathway. *Struct. Folding Des. 7*, 977–988.
30. Brownlee, J., Kayunta, J.-W., Harrison, D. H. T., and Moran, G. R. (2004) The structure of the ferrous form of (4-hydroxyphenyl)-pyruvate dioxygenase from *Streptomyces avermitilis* in complex with the therapeutic herbicide, NTBC. *Biochemistry 43*, 6370–6377.
31. Fritze, I. M., Linden, L., Freigang, J., Auerbach, G., Huber, R., and Steinbacher, S. (2004) The crystal structures of *Zea mays* and *Arabidopsis* 4-hydroxyphenylpyruvate dioxygenase. *Plant Physiol. 134*, 1388–1400.
32. Yang, C., Pflugrath, J. W., Camper, D. L., Foster, M. L., Pernich, D. J., and Walsh, T. A. (2004) Structural basis for herbicidal inhibitor selectivity revealed by comparison of crystal structures of plant and mammalian 4-hydroxyphenylpyruvate dioxygenases. *Biochemistry 43*, 10414–10423.
33. Glasoe, P. K., and Long, F. A. (1960) Use of glass electrodes to measure acidities in deuterium oxide. *J. Phys. Chem. 64*, 188–189.